DOI: 10.1021/ic801864z

Inorganic Chemistry
Article

Multifrequency EPR Studies of $[Cu^{1.5}Cu^{1.5}]^+$ for $Cu_2(\mu\text{-}NR_2)_2$ and $Cu_2(\mu\text{-}PR_2)_2$ Diamond Cores

Neal P. Mankad,[†] Seth B. Harkins,[‡] William. E. Antholine,[§] and Jonas C. Peters*[,†]

[†]*Department of Chemistry, Massachusetts Institute of Technology, Cambridge Massachusetts 02139,* [‡]*Department of Chemistry, California Institute of Technology, Pasadena California 91125, and* [§]*Department of Biophysics, Medical College of Wisconsin, Milwaukee, Wisconsin 53226*

Received September 30, 2008

Multifrequency electron paramagnetic resonance (EPR) spectroscopy is used to explore the electronic structures of a series of dicopper complexes of the type $\{(LXL)Cu\}_2^+$. These complexes contain two four-coordinate copper centers of highly distorted tetrahedral geometries linked by two $[LXL]^-$ ligands featuring bridging amido or phosphido ligands and associated thioether or phosphine chelate donors. Specific chelating $[LXL]^-$ ligands examined in this study include bis(2-*tert*-butylsulfanylphenyl)amide (SNS), bis(2-di-*iso*-butylphosphinophenyl)amide (PNP), and bis(2-di-*iso*-propylphosphinophenyl)phosphide (PPP). To better map the electronic coupling to copper, nitrogen, and phosphorus in these complexes, X-, S-, and Q-band EPR spectra have been obtained for each complex. The resulting EPR parameters implied by computer simulation are unusual for typical dicopper complexes and are largely consistent with previously published X-ray absorption spectroscopy and density functional theory data, where a highly covalent $\{Cu_2(\mu\text{-}XR_2)_2\}^+$ diamond core has been assigned in which removal of an electron from the neutral $\{Cu_2(\mu\text{-}XR_2)_2\}$ can be viewed as ligand-centered to a substantial degree. To our knowledge, this is the first family of dicopper diamond core model complexes for which the compendium of X-, S-, and Q-band EPR spectra have been collected for comparison to Cu_A.

Introduction

A long-standing subject of interest in the field of bioinorganic chemistry concerns the mode by which metalloenzymes mediate electron transfer (ET).[1,2] This is especially true of enzymes that feature redox-active copper centers that serve as ET relays, such as the type 1 sites in blue copper proteins[3−5] and the Cu_A sites of cytochrome *c* oxidases and nitrous oxide reductases. To mediate rapid ET, the local geometry of the copper center(s) must undergo rather little structural change during a redox event so as to minimize the reorganizational term λ,[6] which when large serves to attenuate rates of ET. Therefore, it is of particular interest to understand how copper centers achieve such low structural reorganization in proteins, and by analogy in small molecule model complexes.[7−10] One hypothesis that has been widely advanced is that of the "entatic" or strained state, whereby it is presumed that in order to minimize λ a protein matrix confers a geometry at the redox active site that is similar to the transition state for the ET reaction, a geometry (and function) that would not be prevalent in the absence of the protein matrix. This hypothesis was first advanced by Vallee and Williams,[11] and various researchers, most notably Rorabacher,[12]

*To whom correspondence should be addressed. E-mail: jcpeters@mit.edu.

(1) (a) Ambundo, E. A.; Yu, Q.; Ochrymowycz, L. A.; Rorabacher, D. B. *Inorg. Chem.* **2003**, *42*, 5267. (b) Kyritsis, P.; Dennison, C.; Ingeldew, W. J.; McFarlane, W.; Sykes, A. G. *Inorg. Chem.* **1995**, *34*, 5370. (c) Groenveld, C. M.; Canters, G. W. *J. Biol. Chem.* **1988**, *263*, 167. (d) Groenveld, C. M.; Dahlin, S.; Reinhammer, B.; Canters, G. W. *J. Am. Chem. Soc.* **1987**, *109*, 3247.

(2) (a) Solomon, E. I.; LaCroix, L. B.; Randall, D. W. *Pure Appl. Chem.* **1998**, *70*, 799. (b) Randall, D. W.; Gamelin, D. R.; LaCroix, L. B.; Solomon, E. I. *J. Biol. Inorg. Chem.* **2000**, *5*, 16.

(3) (a) Guss, J. M.; Freeman, H. C. *J. Mol. Biol.* **1983**, *169*, 521. (b) Gray, H. B.; Malmstrom, B. G.; Williams, R. J. P. *J. Biol. Inorg. Chem.* **2000**, *5*, 551.

(4) Shibata, N.; Inoue, T.; Nagano, C.; Nishio, N.; Kohzuma, T.; Onodera, K.; Yoshizaki, F.; Sugimura, Y.; Kai, Y. *J. Biol. Chem.* **1999**, *274*, 4225.

(5) Suzuki, S.; Kataoka, K.; Yamaguchi, K.; Inoue, T.; Kai, Y. *Coord. Chem. Rev.* **1999**, *192*, 245.

(6) Marcus, R. A.; Sutin, N. *Biochim. Biophys. Acta* **1985**, *811*, 265.

(7) (a) Houser, R. P.; Young, V. G.Jr.; Tolman, W. B. *J. Am. Chem. Soc.* **1996**, *118*, 2101. (b) Blackburn, N. J.; deVries, S.; Barr, M. E.; Houser, R. P.; Tolman, W. B.; Sanders, D.; Fee, J. A. *J. Am. Chem. Soc.* **1997**, *119*, 6135. (c) Hagadorn, J. R.; Zahn, T. I.; Que, L.Jr.; Tolman, W. B. *J. C. S. Dalton Trans.* **2003**, 1790.

(8) Al-Obaidi, A.; Baranovič, G.; Coyle, J.; Coates, C. G.; McGarvey, J. J.; McKee, V.; Nelson, J. *Inorg. Chem.* **1998**, *37*, 3567.

(9) (a) LeCloux, D. D.; Davydov, R.; Lippard, S. J. *Inorg. Chem.* **1998**, *37*, 6814. (b) LeCloux, D. D.; Davydov, R.; Lippard, S. J. *J. Am. Chem. Soc.* **1998**, *120*, 6810. (c) He, C.; Lippard, S. J. *Inorg. Chem.* **2000**, *39*, 5225.

(10) Gupta, R.; Zhang, Z. H.; Powell, D.; Hendrich, M. P.; Borovik, A. S. *Inorg. Chem.* **2002**, *41*, 5100.

(11) Vallee, B. L.; Williams, R. J. P. *Proc. Natl. Acad. Sci. U. S. A.* **1968**, *59*, 498.

(12) Rorabacher, D. B. *Chem. Rev.* **2004**, *104*, 651.

Published on Web 07/02/2009

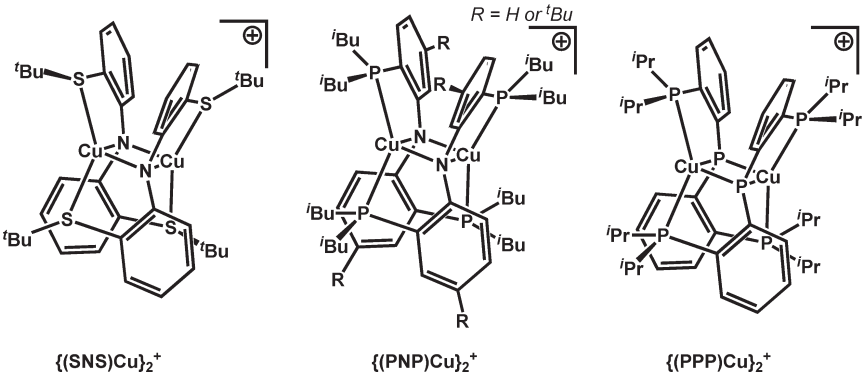

Figure 1. $Cu_2(\mu\text{-}XR_2)_2$ diamond core systems featured in the present study.

have sought small molecule model systems to explore the viability of this approach.

An alternative explanation as to how copper-containing enzymes mediate rapid ET concerns their intimate electronic structures, and the role that metal−ligand covalency plays in providing stabilized electronic states, as opposed to a geometrically strained state. Solomon and co-workers have been among those advancing this idea,[13] both in type-1 copper enzymes and also in Cu_A, in which short and highly covalent Cu−S bonds are prevalent.

Efforts in our laboratories have focused on the preparation of small molecule model complexes that feature the $Cu_2(\mu\text{-}XR_2)_2$ diamond core motif.[14−17] These complexes contain two four-coordinate copper centers of highly distorted tetrahedral geometries linked by two bridging XR_2^- ligands (XR_2^- = NR_2^- or PR_2^-), where the R groups provide neutral donor groups (e.g., thioether or phosphine) to complete the copper coordination spheres. To date, the three systems shown in Figure 1 have been reported.[14−17] A common feature of each of these systems is a fully reversible one-electron redox couple between the reduced dicopper(I,I) state and a one-electron oxidized fully delocalized mixed-valence dicopper(1.5,1.5) state. In this regard, each system is a good functional model of Cu_A. Indeed, the rate of electron self-exchange can be very rapid ($> 10^7\ M^{-1}\ s^{-1}$), as has been estimated for the $\{(SNS)Cu\}_2$ system by NMR line-broadening analysis ((SNS) = bis(2-*tert*-butylsulfanylphenyl)-amide; see Figure 1).[14] X-ray diffraction studies have established that the overall structural reorganization between each set of redox pairs is small. This is especially true of $Cu_2(\mu\text{-}NR_2)_2$ systems supported by the (SNS) and (PNP) ligands, where (PNP) represents the bis(2-di-*iso*-butylphosphinophenyl)amide ligand.[14,17] In these cases, the most noteworthy structural change pertains to a Cu···Cu compression of ∼ 0.15 Å upon one-electron oxidation of the dicopper(I,I) state. This compression is far more pronounced for the (PPP) system (> 0.5 Å),[15] where (PPP) =bis-(2-di-*iso*-propylphosphinophenyl)phosphide.

A recent comparative X-ray crystallography, X-ray absorption spectroscopy (XAS), and density functional theory (DFT) study of the series of compounds $\{(^t\text{Bu-PNP})Cu\}_2^{n+}$ and $\{(PPP)Cu\}_2^{n+}$ (where $n = 0, 1, 2$; ^{t}Bu-PNP = bis-(2-di-*iso*-butylphosphino-5-*tert*-butylphenyl)amide) sought to establish the role played by the bridging X and Cu atoms during successive oxidations. On the basis of that study,[17] it was inferred that a substantial degree of ligand oxidation was prevalent. Indeed, a majority of oxidation occurs at the bridging diarylamido or diarylphosphido units compared with the copper centers, though there is appreciable copper d character in the redox-active molecular orbitals (RAMOs). What is very clear is that the $Cu_2(\mu\text{-}XR_2)_2$ diamond core is a highly covalent unit, and one cannot decouple the oxidation of the metal or bridging atoms from one another. This scenario is also true of the Cu_A site, where it has been estimated that the RAMO in the $Cu_2(\mu\text{-}SR)_2$ mixed-valence state is ∼46% sulfur and ∼44% copper.[13]

To more fully develop the electronic structure description of these redox-active diamond core dicopper systems, we undertook electron paramagnetic resonance (EPR) studies of the formally $Cu^{1.5}Cu^{1.5}$ complexes. Whereas initial studies reported their X-band EPR spectra,[14−16] a detailed analysis of the convoluted spectra had not yet been performed. To aid such an analysis, we have now collected comparative Q-, X-, and S-band EPR spectra for each system shown in Figure 1. This set of data is unique for dicopper model systems and allows for the possibility of quantifying hyperfine interactions between various centers and the unpaired spin, critical in describing their electronic structures and for comparison to published XAS and DFT studies and related data available for Cu_A. Indeed, deconvolution of the EPR parameters by computer simulation reveals values unusual for typical dicopper systems and consistent with a large degree of Cu-XR_2 spin delocalization.

Experimental Section

Dicopper complexes were prepared according to previously published procedures,[14−17] as their $B[3,5\text{-}(CF_3)_2C_6H_3]_4$ salts and EPR spectra were recorded on frozen glasses in 2-methyltetrahydrofuran (5 mM). EPR spectra were obtained at the National Biomedical EPR Center in Milwaukee using Varian E-9 and E109 spectrometers operating at 9 GHz

(13) (a) Gamelin, D. R.; Randall, D. W.; Hay, M. T.; Houser, R. P.; Mulder, T. C.; Canters, G. W.; de Vries, S.; Tolman, W. B.; Lu, Y.; Solomon, E. I. *J. Am. Chem. Soc.* **1998**, *120*, 5246. (b) George, S. D.; Metz, M.; Szilagyi, R. K.; Wang, H. X.; Cramer, S. P.; Lu, Y.; Tolman, W. B.; Hedman, B.; Hodgson, K. O.; Solomon, E. I. *J. Am. Chem. Soc.* **2001**, *123*, 5757. (c) Szilagyi, R. K.; Lim, B. S.; Glaser, T.; Holm, R. H.; Hedman, B.; Hodgson, K. O.; Solomon, E. I. *J. Am. Chem. Soc.* **2003**, *125*, 9158.
(14) Harkins, S. B.; Peters, J. C. *J. Am. Chem. Soc.* **2004**, *126*, 2885.
(15) Mankad, N. P.; Rivard, E.; Harkins, S. B.; Peters, J. C. *J. Am. Chem. Soc.* **2005**, *127*, 16032.
(16) Harkins, S. B.; Peters, J. C. *J. Am. Chem. Soc.* **2005**, *127*, 2030.
(17) Harkins, S. B.; Mankad, N. P.; Miller, A. J. M.; Szilagyi, R. K.; Peters, J. C. *J. Am. Chem. Soc.* **2008**, *130*, 3478.

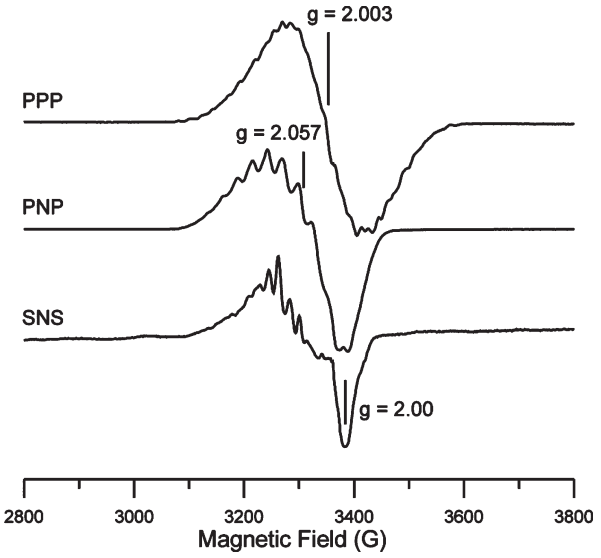

Figure 2. X-band EPR spectra of $\{(PPP)Cu\}_2^+$, $\{(PNP)Cu\}_2^+$, and $\{(SNS)Cu\}_2^+$.

(X band), 3.3 GHz (S band), and 35 GHz (Q band). The low-frequency 3.3 GHz (S band) spectrometer is based on the loop-gap resonator designed by Froncisz and Hyde.[18] The Q-band bridge was modified with the addition of a GaAs field-effect transistor signal amplifier and low-noise Gunn diode oscillator.[19] Microwave frequencies were measured with an EIP model 331 counter. Simulations were carried out using the program Xsophe (Bruker). Xsophe simulations were calculated using matrix diagonalization. Unless otherwise indicated, simulations assumed hyperfine interactions of the unpaired electron with two equivalent Cu atoms, two equivalent bridging (N or P) atoms, and two equivalent nonbridging P atoms where available (vide infra).

Spectrometer conditions were as follows. Q band: microwave power 36 dB; temperature 16.7 K; mod. amplitude 5G set [actual about 3 G]; time constant 0.1 s; 100 kHz mod. frequency; scan time 4 min; microwave frequencies 35.011 GHz (PPP), 35.0008 GHz (SNS), and 35.028 GHz (PNP). S band: microwave power 22 dB; temperature −140 °C; mod. amplitude 5 set [actual about 3 G]; time constant 0.064 s; scan time 2 min; microwave frequencies 3.3661 GHz (SNS), 3.3642 GHz (PNP), and 3.3416 GHz (PPP). X band: microwave power 16 dB; temperature 120 K; mod. amplitude 5 G; time constant 0.128 s; scan time 4 min; microwave frequencies 9.434 GHz (PPP), 9.431 GHz (PNP), and 9.457 GHz (SNS).

Results

X- and Q-Band EPR Spectra of $\{(PPP)Cu\}_2^+$, $\{(PNP)Cu\}_2^+$, and $\{(SNS)Cu\}_2^+$. X-band EPR spectra for the mixed valence compounds $\{(PPP)Cu\}_2^+$,[15] $\{(PNP)Cu\}_2^+$,[16] and $\{(SNS)Cu\}_2^+$[14] are similar to spectra recorded previously (Figure 2, Table 1).[20] The g values are more apparent from the Q-band (35 GHz) spectra (Figure 3, Table 1). The g_{min} values determined from the Q band can then be used for X-band simulations. The hyperfinefine structure in the Q-band spectrum for $\{(PPP)Cu\}_2^+$ is still resolved, indicating that there is little g strain. Neither g_{max} nor g_{min} is separated from the center g value for $\{(PPP)Cu\}_2^+$, consistent with an isotropic g value at this resolution. A high field line for g_{min} in the Q-band spectra for $\{(PNP)Cu\}_2^+$ and $\{(SNS)Cu\}_2^+$ is separated (Figure 3). This high field g value is apparent in the X-band spectrum for $\{(SNS)Cu\}_2^+$, but not as apparent for $\{(PNP)Cu\}_2^+$ or $\{(PPP)Cu\}_2^+$ (Figure 2). The hyperfine structure is not resolved in the Q-band spectra for $\{(PNP)Cu\}_2^+$ and $\{(SNS)Cu\}_2^+$ where g strain contributes to the broadening of the lines.

S-Band Spectra of $\{(PPP)Cu\}_2^+$, $\{(PNP)Cu\}_2^+$, and $\{(SNS)Cu\}_2^+$. The hyperfine structure in the EPR signatures for $\{(PPP)Cu\}_2^+$, $\{(PNP)Cu\}_2^+$, and $\{(SNS)Cu\}_2^+$ is better resolved in their low-frequency S-band spectra (Figure 4). Additional lines in the S-band spectrum for $\{(PNP)Cu\}_2^+$ are resolved on the high-field side where there are only inflections in the X-band spectrum (Figure 2). The g value close to the crossover point in Figure 4 is g_{iso} for $\{(PPP)Cu\}_2^+$ and is close to g_{mid} for $\{(PNP)Cu\}_2^+$ and $\{(SNS)Cu\}_2^+$, as taken from the Q-band data. The g anisotropy is not as evident at the S band because the g values are getting closer, as determined by field position. Using the g value determined for $\{(SNS)Cu\}_2^+$ and $\{(PNP)Cu\}_2^+$ at the Q band, g_{mid} is determined in the center of the spectrum. Equally spaced lines around g_{mid} are the hyperfine lines. There should be a 1:2:3:4:3:2:1 seven-line pattern centered at g_{mid} if the hyperfine lines are only from two coppers. The observed 11 lines are consistent with a 1:4:10:20:26:28:26:20:10:4:1 pattern for $\{Cu_2(\mu\text{-}NR_2)_2\}^+$, where the hyperfine couplings are about equal for copper and nitrogen (Figures 2 and 4).

Second-Derivative Multifrequency EPR Spectra and Simulations for $\{(PPP)Cu\}_2^+$. The second derivative of an EPR spectrum emphasizes sharp lines and de-emphasizes broad lines. Of the three complexes described in this paper, the hyperfine lines for $\{(PPP)Cu\}_2^+$ are most apparent and easiest to compare at X-, Q-, and S-band frequencies (Figure 5). The spectra are centered at the apparent, to first-order, isotropic g value, 2.003. The large number of resolved lines in the X- and S-band spectra of each species, most apparent in the second-derivative spectra for $\{(PPP)Cu\}_2^+$ in Figure 5, suggests that the hyperfine lines do not arise from copper alone. Two almost equivalent coppers in $\{(PPP)Cu\}_2^+$ are expected to give seven lines for each g value. If the lines are from more than one g value, they should not line up at three different microwave frequencies. About 20 lines are almost aligned at the three frequencies. This indicates that the hyperfine lines are due to not only Cu ($I = 3/2$) but also P (I=1/2), assuming that the copper hyperfine lines are from equivalent coppers and not inequivalent coppers with different hyperfine values, in accord with previous XRD studies.[15] The lines are better resolved as the frequency is lowered. Moreover, almost all of the hyperfine lines line up at all three frequencies. At the higher frequencies, the relative intensities are not evident due to line broadening and partial overlap of the lines. At the S band, the lines are so well resolved that the relative intensity of the lines becomes more evident. For example, on the low-field side of the spectrum, some of

(18) Froncisz, W.; Hyde, J. S. *J. Magn. Reson.* **1982**, *47*, 515.
(19) Hyde, J. S.; Newton, M. E.; Strangeway, R. A.; Camenisch, T. G.; Froncisz, W. *Rev. Sci. Instrum.* **1991**, *62*, 2969.
(20) The experimental X-band EPR spectrum of $\{(PNP)Cu\}_2^+$ has not been previously published. The experimental X-band spectrum of $\{(SNS)Cu\}_2^+$ can be found in ref 14, and that for $\{(PPP)Cu\}_2^+$ can be found in the Supporting Information of ref 15.

Table 1. EPR Parameters for $\{(LXL)Cu\}_2^+$ from Simulations and Comparative Literature Values for Cu_A and the Mixed-Valence Complex Cu_2L[a]

	g_{max}	g_{mid}	g_{min}	A_{max}^{Cu}	A_{mid}^{Cu}	A_{min}^{Cu}	A_{max}^{b}	A_{mid}^{b}	A_{min}^{b}	A^c
$\{(PPP)Cu\}_2^+$		2.00			45 G			45 G		12.5 G
$\{(PNP)Cu\}_2^+$	2.08	2.06	2.00	~40 G	27 G	15 G	~12 G	24 G	15 G	~5 G
$\{(SNS)Cu\}_2^+$	2.07	2.06	2.00	~44 G	17 G	~5 G	~12 G	17 G	~ 5 G	
Cu_A	2.180	2.024	2.007	40 G	21 G	21 G				5.6 G
Cu_2L	2.15	2.15	2.02	103 G	103 G	21 G				5−9 G

[a] L is $(N[CH_2CH_2N(H)CH_2CH_2N(H)CH_2CH_2]_3N)$, ref 22; $A^{N'}$ taken from ref 23. EPR parameters for A^{Cu} for Cu_A corrected for ^{63}Cu instead of ^{65}Cu, as given in the ref 5. Values were averaged for $A^{Cu(1)}$ and $A^{Cu(2)}$ for Cu_A. An isotropic g value for PPP is assumed. The g value is taken as the crossover point in the Q-band spectrum, but the crossover point moves to 2.014 at the X-band and 2.055 at the S band. Since g_{min} and g_{mid} are not resolved in the Q-band spectrum, an error of ±0.02 is assumed. For g_{min}, the high-field sharp line in the spectra for SNS, the calculated g values are 2.001 for the S band, 1.998 for the X band, and 1.990 for the Q band. The g_{min} for SNS is set to 2.00 ± 0.01. The g values were calibrated using DPPH. [b] This hyperfine value is attributed to the bridging N or P atom. [c] This superhyperfine value is attributed to the nonbridging P or N donor.

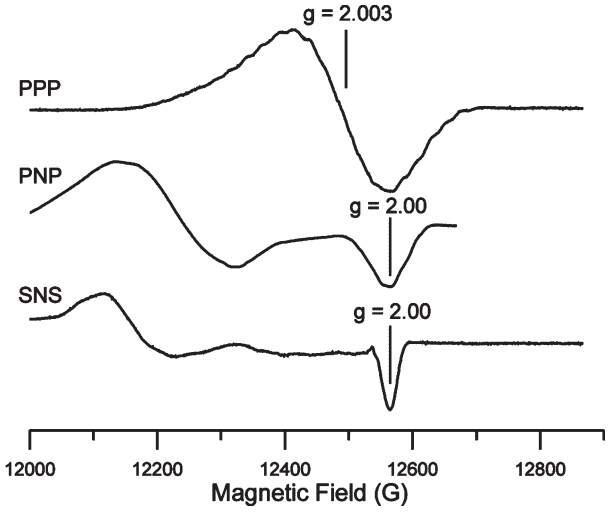

Figure 3. Q-band EPR spectra of $\{(PPP)Cu\}_2^+$, $\{(PNP)Cu\}_2^+$, and $\{(SNS)Cu\}_2^+$.

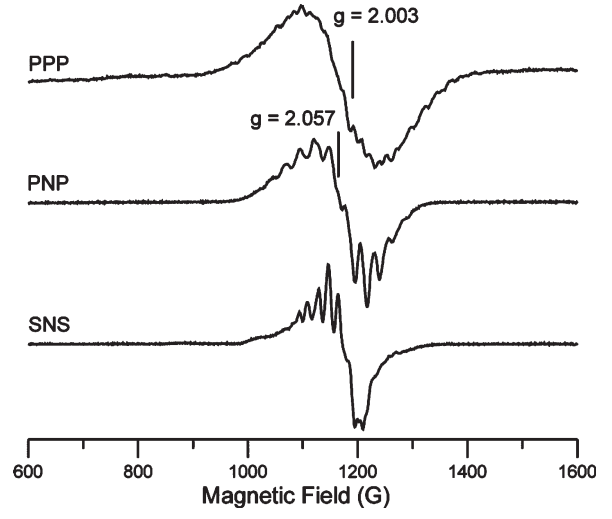

Figure 4. S-band EPR spectra of $\{(PPP)Cu\}_2^+$, $\{(PNP)Cu\}_2^+$, and $\{(SNS)Cu\}_2^+$.

the lines have relative intensities of 1:2:1, consistent with coupling to two almost equivalent nuclei with $I = 1/2$, that is, a pattern due to two almost equivalent P atoms (Figure 5, circled area). Assiging the 1:2:1 pattern to two almost equivalent P atoms gives $A^{P(terminal)} = 12.5$ G. The next three lines also form a 1:2:1 pattern. The difference

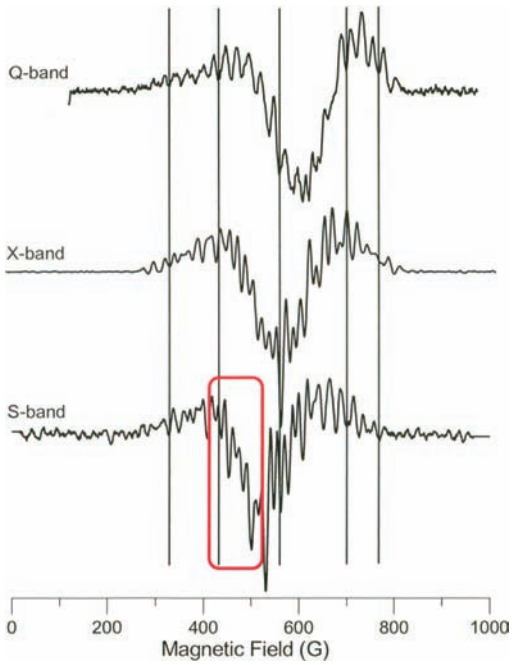

Figure 5. Second derivative of Q-, X-, and S-band spectra for $\{(PPP)Cu\}_2^+$.

in field for the centers of both 1:2:1 patterns gives a second hyperfine value assigned to copper and phosphorus, that is, $A^{Cu} \sim A^{P(bridge)} = 45$ G. Note that a 1:4:6:4:1 pattern is expected for four equivalent P atoms, and it is difficult to distinguish between a 1:2:1 and a 4:6:4 pattern where the lines with intensity 1 are superimposed onto more-intense lines. It is also possible that geometric factors dictate inequivalent coupling of the unpaired spin to the terminal phosphines, much like coupling that is observed with the CH_2 protons in the tyrosine radical in ribonucleotide reductase.[21] Simulation of the spectra with $A^{Cu} = 45$ G, $A^{P(bridge)} = 45$ G, and $A^{P(terminal)} = 12.5$ G and a line width of 5 G gives a multiline pattern that is better resolved than the experimental S-band spectrum for $\{(PPP)Cu\}_2^+$ because the line width is less for the simulation than for the experimental spectrum

(21) (a) Sjoberg, B.-M.; Peichard, P.; Graslund, A.; Ehrenberg, A. *J. Biol. Chem.* **1977**, *252*, 536. (b) Graslund, A.; Sahlin, M.; Sjoberg, B.-M. *Environ. Health Perspect.* **1985**, *64*, 139.
(22) Barr, M. E.; Smith, P. H.; Antholine, W. E.; Spencer, B. *J. Chem. Soc. Chem. Commun.* **1993**, 1649.
(23) Kababya, S.; Nelson, J.; Calle, C.; Neese, F.; Goldfarb, G. *J. Am. Chem. Soc.* **2006**, *128*, 2017.

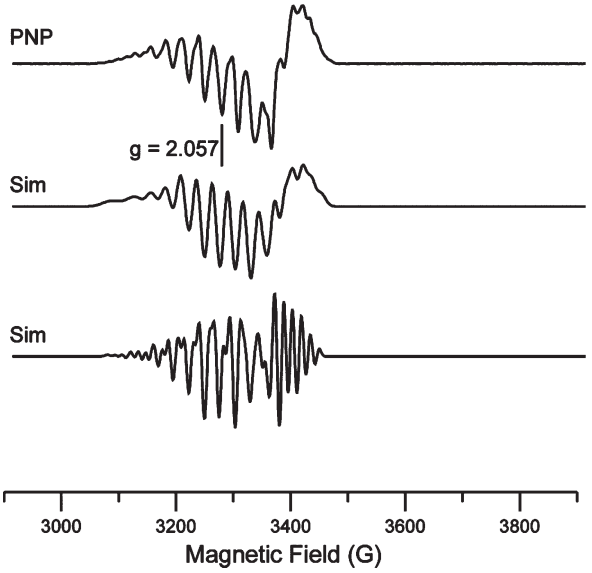

Figure 6. Second-derivative X-band spectrum for $\{(PNP)Cu\}_2^+$ and simulations. EPR parameters for simulations: g_{max}, g_{mid}, and g_{min} are 2.085, 2.057, and 2.000; A_{max}^{Cu}, A_{mid}^{Cu}, A_{min}^{Cu} are 40, 27, and 15 G; A_{max}^{N}, A_{mid}^{N}, and A_{min}^{N} are 12, 24, and 15 G; line widths are 15, 11, and 10 G (top simulation) and 5, 5, and 5 G (bottom simulation); microwave frequency, 9.434 GHz.

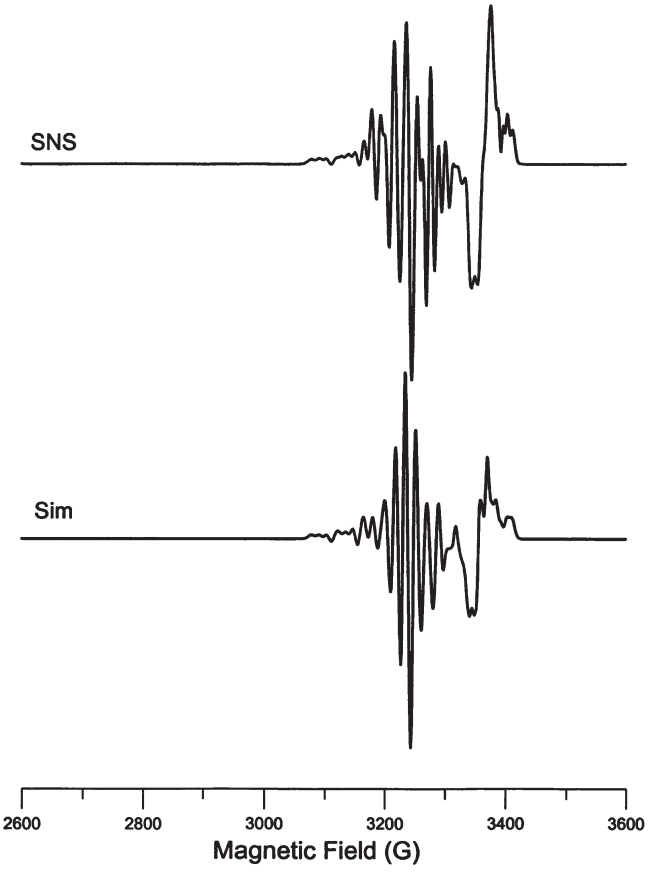

Figure 7. Second-derivative X-band spectrum for $\{(SNS)Cu\}_2^+$ and simulation. EPR parameters for simulation: g_{max}, g_{mid}, and g_{min} are 2.069, 2.066, and 2.00; A_{max}^{Cu}, A_{mid}^{Cu}, and A_{min}^{Cu} are 44, 17, and 5 G; A_{max}^{N}, A_{mid}^{N}, and A_{min}^{N} are 12, 17, and 5 G; line widths are 7, 7, and 4 G; microwave frequency, 9.377 GHz.

(Supporting Information Figure S1). The number of lines and the splitting of the lines in the simulation are similar to the lines in the experimental spectrum. A limitation of this simulation is that the variables are underdetermined. The g and A axes are taken as coincident with all Euler angles at zero. M_I-dependent line width parameters and quadruple terms were not used. The simulation is thus consistent with, but not proof of, the values for the experimental spectrum.

Second-Derivative EPR Spectra and Simulations for $\{(PNP)Cu\}_2^+$ and $\{(SNS)Cu\}_2^+$. The X-band spectrum for $\{(PNP)Cu\}_2^+$ (Figure 2) has 10 clearly resolved lines in the center of the spectrum, which is attributed to the g_{mid} region. The resolved lines for $\{(PNP)Cu\}_2^+$ are broader than the lines for $\{(SNS)Cu\}_2^+$, presumably due to the superhyperfine lines from the terminal P atoms. Initial simulation of a single isotropic line with a line width of 6 G and subsequent addition of hyperfine lines for two phosphorus atoms with $A^{P(terminal)} = 5$ G doubles the peak-to-peak width from 7 to 15 G (data not shown). It is estimated that $A^{P(terminal)} \sim 5$ G from this simulation of the single line. If four phosphorus atoms are almost equivalent, $A^{P(terminal)}$ should be slightly less than 5 G. The second derivative of this spectrum emphasizes the lines that are resolved (Figure 6). Since only seven lines for the g_{mid} region are expected for the copper hyperfine from a class III mixed-valence complex, hyperfine lines from nitrogen were considered to increase the number of lines. Simulation of the Q-band data, which is the most sensitive to g values, provided the rhombic tensors g_{max}, g_{mid}, and g_{min} of 2.085, 2.060, and 2.000, respectively (Supporting Information Figure S2). A good simulation of the X-band spectrum for $\{(PNP)Cu\}_2^+$ can then be obtained with g_{max}, g_{mid}, and g_{min} values of 2.085, 2.057, and 2.000; A^{Cu} values of 40, 27, and 15 G; and A^{N} values of 12, 24, and 15 G (Figure 6). The S-band spectrum may also be fit using these parameters (Supporting Information Figure S3), lending weight to their assignments.

As already noted, the X-band EPR spectrum of $\{(SNS)Cu\}_2^+$ has been published, and a crude simulation is consistent with a class III mixed-valence species.[20] As for $\{(PPP)Cu\}_2^+$, second-derivative spectra for $\{(SNS)Cu\}_2^+$ emphasize the sharp features in the spectra (Figure 7). The lines and line shapes in the high-field and low-field regions are consistent with rhombic g values. There are about 10 lines in the center of the spectrum, which comprise the g_{mid} region. Assuming more than seven lines in the g_{mid} region, a seven-line pattern for Cu(1.5)Cu(1.5) does not fit the experimental spectrum. Thus, superhyperfine lines are observed involving splittings from, presumably, the bridging nitrogens. Using EPR parameters from Q-, X-, and S-band spectra, a simulation with g_{max}, g_{mid}, and g_{min} equal to 2.069, 2.066, and 2.00; A^{Cu} values of 44 G, 17 G, and 5 G; and A^{N} values of 12 G, 17 G, and 5 G fits the experimental spectrum extremely well (Figure 7). While simulations are consistent with, not proof of, the EPR parameters, the EPR experimental and simulated parameters do appear to be very close. One criterion for the goodness of fit is to simulate at another frequency without changing the EPR parameters. The simulation of the S-band spectrum is equally good, thus increasing the confidence in the EPR parameters (Figure 4).

Table 2. Estimated Spin Density Distribution from DFT Calculations

Cu_A[24]	38% Cu	44% bridging S		
$\{(PPP)Cu\}_2^{+}$[17]	18% Cu	44% bridging P	14% terminal P	22% C and H
$\{(^tBu\text{-}PNP)Cu\}_2^{+}$[17]	16% Cu	35% bridging N	11% terminal P	38% C and H

Discussion

Asymmetry in the coordination environment of the copper centers for $\{(^tBu_2\text{-}PNP)Cu\}_2^{+}$ and $\{(^tBu_2\text{-}PNP)Cu\}_2^{2+}$ has been observed via solid-state XRD analysis and is presumably a phenomenon specific to the solid-state.[17] Similar asymmetry was not observed for the (SNS)- and (PPP)-supported systems in the solidstate.[14,15] For completeness, and direct comparison to the EPR data presented here, the solid-state X-ray structure of $\{(PNP)Cu\}_2^{+}$ has also been determined and placed in the Supporting Information. It shows substantial asymmetry about the diamond core motif akin to $\{^tBu_2\text{-}(PNP)Cu\}_2^{+}$. In solution or upon freezing to a glass, however, $\{(PNP)Cu\}_2^{+}$ is a fully delocalized, class-III mixed valence species based upon the EPR data available.

Cu_A has g values of $g_{min} = 2.007$, $g_{mid} = 2.024$, and $g_{max} = 2.180$ (Table 1).[24] For Cu_A, $g_{max} > g_{mid} \sim g_{min}$, and the ground state for the coppers is primarily $d_{x^2-y^2}$. A g value close to 2.00 for Cu_A suggests admixture of a low-lying excited state. This unusual behavior is also evident in our model compounds. For $\{(SNS)Cu\}_2^{+}$, $g_{min} = 2.00$, $g_{mid} = 2.066$, and $g_{max} = 2.069$. The ground state for the coppers involves the d_{z^2} orbitals more than the $d_{x^2-y^2}$ orbitals, as reflected by $g_{\perp} > g_{\parallel}$ where g_{mid} and g_{max} are $g_{\perp}$. For $\{(PNP)Cu\}_2^{+}$, $g_{min} = 2.00$, $g_{mid} = 2.055$, and $g_{max} = \sim 2.08$. Here the g values are rhombic. In contrast, for $\{(PPP)Cu\}_2^{+}$ only one g value from the crossover point, 2.003, is assigned as the signal is nearly isotropic at the resolutions we have achieved.

The line widths of the spectra in Figure 2 are consistent with sharp lines for $\{(SNS)Cu\}_2^{+}$, which have only copper and nitrogen hyperfine lines. For $\{(PNP)Cu\}_2^{+}$, the hyperfine lines are broader, consistent with an additional superhyperfine contribution from nonbridging phosphorus. A key feature for the spectrum of $\{(PPP)Cu\}_2^{+}$ is the increase in the number of hyperfine lines, which are assigned to copper and bridging phosphorus atoms, where an increase in line width accounts for terminal phosphorus atoms.

The interpretation of the hyperfine and superhyperfine structure is simplest for $\{(SNS)Cu\}_2^{+}$ because there are no superhyperfine couplings from the terminal ligands. The lowest-field lines in the spectrum (Figure 7) are separated from the other lines, equivalent to lines expected in a single crystal, and well-simulated with $g_{max} = 2.069$, $A_{max}^{Cu} = 44$ G, and $A_{max}^{N} = 12$ G. The **g** and **A** tensors in the simulation are coincident, but it is not known how sensitive the spectra are to the Euler angles. The number of lines in the g_{mid} region is similar in both the experimental g_{mid} region and the simulated spectrum (Figure 7). It is concluded that there are more than seven lines in the g_{mid} region, which implies hyperfine lines from both copper and nitrogen. A crude simulation assuming a seven-line pattern for equivalent coppers has been published[20] but does not fit nearly as well as the simulation shown in Figure 7. The shape of the lines for g_{min} in the high-field region are not as close to the experimental spectrum as those of the lines for the g_{max} and g_{mid} regions, but other than the line width being narrow, little information about the parameters was gained from the experimental spectrum (Figure 7). Simulation parameters for the g_{min} region are $g_{min} = 2.00$, $A_{min}^{Cu} = 5$ G, and $A_{min}^{N} = 5$ G. A_{min}^{Cu} and A_{min}^{N} are much less than the parameters for A_{max} and A_{mid}, and hence the tensors are anisotropic. A^N for a terminal nitrogen is expected to be more isotropic. The anisotropic values for A^N for $\{(SNS)Cu\}_2^{+}$ and $\{(PNP)Cu\}_2^{+}$ thus appear to be characteristic for the bridging N atoms. The isotropic values for $A^{P(bridging)}$ for $\{(PPP)Cu\}_2^{+}$ are approximate values because the g values are quenched, making assignments for the x, y, and z directions more difficult, and because the time to simulate with anisotropic values was prohibitive. Therefore, the degree of anisotropy for $A^{P(bridging)}$ for $\{(PPP)Cu\}_2^{+}$ was not determined. Curiously, despite greater calculated Cu spin density in Cu_A relative to the $\{(LXL)Cu\}_2^{+}$ model compounds (Table 2), the values for A^{Cu} are more or less similar to the values for A^{CuA}, with A^{Cu} for $\{(PPP)Cu\}_2^{+}$ somewhat greater than for A^{CuA} and with A^{Cu} for $\{(PNP)Cu\}_2^{+}$ and $\{(SNS)Cu\}_2^{+}$ about the same or somewhat less than for A^{CuA}. It may be that the value for A^{Cu} for $\{(PPP)Cu\}_2^{+}$ is not isotropic but anisotropic, and the anisotropy in the EPR spectrum is not readily evident. In this case, the spin density for Cu would be overestimated.

Recently, XAS and electronic structure calculations were obtained for $\{(PNP)Cu\}_2^{n+}$ ($n = 0,1,2$) and $\{(PPP)Cu\}_2^{n+}$.[17] Rhee and Head-Gordon have independently undertaken a theoretical study of $\{(PPP)Cu\}_2^{n+}$.[25] It has generally been concluded that the redox chemistry for $\{(PPP)Cu\}_2^{n+}$ and $\{(^tBu_2\text{-}PNP)Cu\}_2^{n+}$ is substantially delocalized throughout the $Cu_2(\mu\text{-}XR_2)_2$ cores, with a majority component of the redox chemistry occurring at the bridging N or P units (Table 2). The values obtained for A^N and $A^{P(bridging)}$ are consistent with this hypothesis. Values from Table 1 for $A^{P(terminal)}$ for $\{(PPP)Cu\}_2^{+}$ of 12.5 G and for $\{(PNP)Cu\}_2^{+}$ of about 5 G are in accord with modest terminal phosphorus contributions. $A^{N(terminal)}$ is 5.6 G for Cu_A (Table 1), but the ratio of the nuclear moments for P to N is 2.26320 to 0.4037607. If the electron densities for the terminal N and phosphorus were similar, a value of about 30 G would be expected for $A^{P(terminal)}$. The electron density on the bridging phosphorus or nitrogen is substantially greater (Table 2) than for the terminal phosphorus, which is in accordance with large bridging atom A values. Moreover, quenching of the g values for $\{(PPP)Cu\}_2^{+}$ to an almost isotropic value together with delocalization of the spin density on the bridging phosphorus suggest the presence of P-centered radical character. A^N values for $\{(PNP)Cu\}_2^{+}$ and $\{(SNS)Cu\}_2^{+}$ (Table 1) are comparable to those observed for N-localized radicals such as Me_2N ($A^N = 14.7$ G)[26] and nitroxide radicals ($A^N \sim 32$ G).[27] P-centered

(24) Neese, F.; Zumft, W. G.; Antholine, W. E.; Kroneck, P. M. H. *J. Am. Chem. Soc.* **1996**, *118*, 8692.

(25) Rhee, Y. M.; Head-Gordon, M. *J. Am. Chem. Soc.* **2008**, *130*, 3878.

(26) Brand, J. C.; Cook, M. D.; Roberts, B. P. *J. Chem. Soc., Perkin Trans. II* **1984**, 1187.

(27) Libertint, L. J.; Griffith, O. H. *J. Chem. Phys.* **1970**, *53*, 1359.

radicals are less common, and A^P values range from 42.5 G in highly delocalized systems[28] to 96.3 G in $P[CH(SiMe_3)_2]_2$.[29] The A^P value in $\{(PPP)Cu\}_2$ (45 G) is in the range expected for free P-centered radicals. Such direct observation of $A^X_{(bridging)}$ in the $Cu_2(\mu\text{-}X)_2$ core of Cu_A is not possible because the bridging S atoms are spin-inactive ($I = 0$).

(28) Agarwal, P.; Piro, N. A.; Meyer, K.; Müller, P.; Cummins, C. C. *Angew. Chem., Int. Ed.* **2007**, *46*, 3111.

(29) Gyanne, M. J. S.; Hudson, A.; Lappert, M. F.; Power, P. P.; Goldwhite, H. *J. Chem. Soc., Dalton Trans.* **1980**, 2428.

Acknowledgment. J.C.P. acknowledges support from the NSF (GOALI). N.P.M. is grateful for an NSF graduate fellowship. W.E.A. acknowledges the National Biomedical EPR Center Grant EB001980 from NIH. The authors are grateful to a reviewer concerning the EPR simulations.

Supporting Information Available: Crystallographic data (CIF) and supporting EPR spectra are available free of charge via the Internet at http://pubs.acs.org.